ORIGINAL ARTICLE

**DOI**: https://doi.org/10.18599/grs.2020.1.4-12

# Pore-scale investigation of the displacement fluid mechanics during two-phase flows in natural porous media under the dominance of capillary forces

*T.R. Zakirov[1*], M.G. Khramchenkov[1,2]*

[1]*Kazan Federal University, Kazan, Russian Federation*

[2]*Scientific Research Institute for System Analysis of the Russian Academy of Sciences, Moscow, Russian Federation*

**Abstract**. This paper presents the results of numerical simulations of two-phase flows in porous media under capillary forces dominance. For modeling of immiscible two-phase flow, the lattice Boltzmann equations with multi relaxation time operator were applied, and the interface phenomena was described with the color-gradient method. The objective of study is to establish direct links between quantitative characteristics of the flow and invasion events, using high temporal resolution when detecting simulation results. This is one of the few works where Haines jumps (rapid invasion event which occurs at meniscus displacing from narrow pore throat to its wide body) are considered in three-dimensional natural pore space, but the focus is also on the displacement mechanics after jumps. It was revealed the sequence of pore scale events which can be considered as a period of drainage process: rapid invasion event during Haines jump; finish of jump and continuation of uniform invasion in current pore; switching of mobile interfaces and displacement in new region. The detected interface change, along with Haines jump, is another distinctive feature of the capillary forces action. The change of the mobile interfaces is manifested in step-like behavior of the front movement. It was obtained that statistical distributions of pressure drops during Haines jumps obey lognormal law. When investigating the flow rate and surface tension effect on the pressure drop statistics it was revealed that these parameters practically don't affect on the statistical distribution and influence only on the magnitude of pressure drops and the number of individual Haines jumps.

**Keywords:** two-phase flow, Haines jumps, capillary forces, lattice Boltzmann equations, color-gradient method, X-ray computed tomography

**Recommended citation**: Zakirov T.R., Khramchenkov M.G. (2020). Pore-scale investigation of the displacement fluid mechanics during two-phase flows in natural porous media under the dominance of capillary forces. *Georesursy = Georesources*, 22(2), pp. 4-12. DOI: https://doi.org/10.18599/grs.2020.1.4-12

## 1. Introduction

Understanding of two-phase flow processes in porous media plays an important role in wide range of scientific and engineering disciplines, such as hydrogeology, oil- and gas-field development, soil science, underground hydromechanics, cardiology, etc. With the development of computing and experimental technique, many modern papers, studying the multiphase flows in porous media, have appeared (Liu et al., 2016; Chen et al., 2018; Zakirov et al., 2018a; Aursjø et al., 2011; Tsuji et al., 2016). These papers are united by the investigation of one phenomenon – the development of instabilities during two-phase drainage flow in porous media. Depending on the mechanics of the instabilities development, three displacement patterns of two-phase flows are distinguished: viscous fingering, capillary fingering and flow with stable front. It was shown in that the instability type is controlled by capillary number (*Ca*) and viscous ratio between non-wetting and wetting fluids (*M*).

The pattern with stable front is observed at simultaneously high *Ca* and $M \geq 1$. This flow is characterized by ideal flat interface in 2D homogeneous models (Liu et al., 2016), but, as shown in (Tsuji et al., 2016), the front geometry in natural heterogeneous porous media is far from stable. The flow with viscous fingering is formed at $M \leq 0.1$ and high *Ca* (typically more than $10^{-3}$). In this regime, viscous forces strongly exceed capillary forces. This flow pattern is characterized by unstable front displacement, the formation of dominant displacement channels directed along the pressure drop, and tree-like structure of the instabilities (Zakirov et al., 2018b; Tsuji et al., 2016).

*Corresponding authors: Timur R. Zakirov
E-mail: tirzakirov@kpfu.ru

© 2020 The Authors. Published by Georesursy LLC
This is an open access article under the Creative Commons Attribution 4.0 License (https://creativecommons.org/licenses/by/4.0/)

At low *Ca* (typically less than $10^{-5}$), capillary forces dominate and the capillary fingering is observed. Some characteristics of such flow type are described in (Zakirov et al., 2018b; Tsuji et al., 2016; Yamabe et al., 2015). However, most of the modern works studying the mechanics of displacement in the regime of dominance of capillary forces are aimed at studying the Haines jumps. This event was first discovered in (Haines et al., 1930) and is characterized by burst-like the meniscus displacement from narrow pore throat to wide pore body, which is accompanied by sharp capillary pressure drop. Hines jumps are a bright example of the capillary forces manifestation in a porous medium.

In (Moebius, Or, 2012, 2014), Haines jumps investigation was performed at controlling of the pressure difference between fluids. Pressure fluctuations were detected during drainage displacement and Haines jumps were associated with sharp pressure drop, but the displacement mechanics after jumps wasn't investigated in detail. The measurement of interfacial velocities during Haines jumps was performed in (Moebius, Or, 2012; Zacharoudiou, Boek, 2016; Armstrong, Berg, 2013; Armstrong et al., 2015). It was shown that the velocity of meniscus displacement many times exceeds bulk flow rate and affect the fluids distribution in adjacent pores. Reynolds number is not negligibly small in that cases. Thus, the inertial forces should not be ignored and, as shown in (Armstrong et al., 2015), the *Ca* and *M* values are not enough for controlling the capillary fingering pattern. The Ohnesorge number which relates the viscous, inertial and capillary forces was offered to use in (Zacharoudiou, Boek, 2016).

In present paper, the displacement mechanics is studied using the mathematical modeling. In recent years, the lattice Boltzmann equations (LBM) is a widely used tool for pore-scale simulations of the two-flow processes (Liu et al., 2016; Zakirov et al., 2018b; Aursjø et al., 2011; Tsuji et al., 2016; Yamabe et al., 2015). In our study, we use the most modern version of the color-gradient method. LBM using the MRT collision operator (MRT – Multi relaxation time) with color gradient model for 3D lattices (D3Q15, D3Q19, and D3Q27) is formulated in (Leclaire et al., 2017)

The objective of this paper is to study the mechanics of two-phase drainage flow under the capillary forces dominance. The originality of the work is the study of events occurring in the porous space after Haines jump as well as the natural character of the pore structure.

We focus on establishing a direct links between quantitative dynamic characteristics of two-phase flow and invasion events, using high temporal resolution when detecting the results.

A special attention is paid to exploration of the statistical distributions of pressure drops which occur during Haines jumps in 3D natural sandstone. The influence of flow rate and surface tension on statistical properties of pressure drops is especially studied.

## 2. Materials and methods

### 2.1. LBE formulation

In the LBE, the fluid flow is considered as dynamics of particles ensemble with a given finite number of possible velocities. The flow domain in standard case is a grid with square or cubic cells. The set of these cells forms a lattice with step $\Delta l$. During a time step $\Delta t$, particles without interaction with each other can make one act of displacement between adjacent nodes. One-particle distribution functions $f(\mathbf{r}, \boldsymbol{u}, t)$ are used to describe the state of the system at each grid node. This function shows the part of particles at time $t$ located in the vicinity of point $\mathbf{r}(x, y, z)$ with coordinates from $x$ to $x+\Delta x$, from $y$ to $y+\Delta y$, from $z$ to $z+\Delta z$ and with velocity range from $\mathbf{u}(u_x, u_y, u_z)$ to $\mathbf{u}(u_x+\Delta u_x, u_y+\Delta u_y, u_z+\Delta u_z)$ (Leclaire et al., 2017).

In this paper, we consider two-dimensional case. Possible directions for particles moving are described using D3Q19 model. Since a detailed description of this model already cited in (Leclaire et al., 2017, Zakirov et al., 2018b), we restrict ourselves to a brief presentation of basic formulas and steps.

The dynamics of the particles ensemble for each fluid is described in several stages. The first is a streaming step. At this stage, during $\Delta t$ the particles move to neighboring nodes in possible for D3Q19 directions. The second stage deals with the particles collision, as a result of which the distribution function tends to an equilibrium state. At the third stage, the phenomena on fluids interface are considered. Evolution of $f_i^k$ in time and space is described by Eq. (1):

$$f_i^k(\mathbf{r}+\mathbf{e}_i\Delta t, t+\Delta t) = f_i^k(\mathbf{r},t) + (\Omega_i^k(\mathbf{r},t))^1 \quad (\Omega_i^k(\mathbf{r},t))^2 \tag{1}$$

where $k = 1, 2$ and indicates fluid type, i.e. wetting and non-wetting phases; $i = (1\text{-}19)$ characterizes the direction of particles movement in D3Q19; $(\Omega_i^k)^1$ is a collision operator, and $(\Omega_i^k)^2$ describes interactions between two fluids.

The macroscopic densities of each fluid and their total velocity are obtained by Eq. (2) and (3):

$$\rho^k(\mathbf{r},t) = \sum_{i=1}^{19} f_i^k(\mathbf{r},t) \tag{2}$$

$$\mathbf{u}(\mathbf{r},t) = \frac{1}{\rho}\sum_{k=1}^{2}\sum_{i=1}^{19}\mathbf{e}_i f_i^k(\mathbf{r},t) \tag{3}$$

Due to more accurate results when using the MRT model (Zakirov et. al, 2018a), in comparison with SRT-model (SRT – Single relaxation time), the first approach is applied in present paper:

$$(\Omega_i^k)^1 = -M^{-1}S(m_i^k - m_i^{k\,eq}) \tag{4}$$

In Eq. (4), $m_i^k = \sum_{j=1}^{19} M_{ij} \cdot f_j^k$. The view of matrix $M$ and formulas for calculation of $m_i^{k\,eq}$, and the components of the diagonal matrix $S$ are described in (Zakirov et. al, 2018a). Set B for matrix $S$ in also shown (Zakirov et. al, 2018a)

Pressure $P^k$ is associated with density by following relation: $P^k = \rho^k c^2/3$, where $c = \Delta l / \Delta t$ – the lattice speed, $\Delta l$ – grid spacing.

The relaxation parameter $\tau^k$ controls the kinematic viscosity $\mu^k$ (Eq. (5)):

$$\mu^k = \left(\frac{2\tau^k - 1}{6}\right)\frac{\Delta l^2}{\Delta t} \quad (5)$$

To describe the phenomena between fluids as well as between fluid and solid phase, the color-gradient method is applied (Leclaire et al., 2017). First, the color-gradient vector **g** is defined as (Leclaire et al., 2017):

$$\mathbf{g}(\mathbf{r},t) = \sum_{i=1}^{19} \mathbf{e}_i(\rho^2(\mathbf{r}+\mathbf{e}_i\Delta t,t) - \rho^1(\mathbf{r}+\mathbf{e}_i\Delta t,t)) \quad (6)$$

The contact wetting angle $\theta$ is simulated in color-gradient method by giving the values of densities to the solid cells.

Next, the perturbation operator $(\Omega_i^k)^2$ is calculated by:

$$(\Omega_i^k)^2 = \frac{A^k}{2}|\mathbf{g}|(w_i \cdot \frac{(\mathbf{e}_i \cdot \mathbf{g})}{|\mathbf{g}|} - B_i) \quad (7)$$

In Eq. (7), $|\mathbf{g}|$ is a module of color-gradient vector; $A^k$ is a numerical parameter which controls a magnitude of surface tension, and it's assumed that $A^1 = A^2 = A$; $B_i$ takes the following values: $B_1 = -2/9$; $B_{2-7} = 1/27$; $B_{8-19} = 1/54$; $w_1 = 1/3$; $w_{2-7} = 1/18$; $w_{8-19} = 1/36$ – the weights coefficients.

Perturbation operator in Eq. (7) models surface tension, but doesn't provide an immiscibility of fluids. For avoidance their mixing, the recoloring operator is used. This step is performed after solving the Eq. (1) with MRT-operator $(\Omega_i^k)^1$ and perturbation operator $(\Omega_i^k)^2$ applying, and consists in modifying of $f_i^k$ (Leclaire et al., 2017):

$$(f_i^1)^* = \frac{\rho^1}{\rho} f_i - \beta \frac{\rho^1 \cdot \rho^2}{\rho} f_i^{eq} \cdot \cos(\alpha_i) \quad (8)$$

$$(f_i^2)^* = \frac{\rho^2}{\rho} f_i + \beta \frac{\rho^2 \cdot \rho^1}{\rho} f_i^{eq} \cdot \cos(\alpha_i) \quad (9)$$

where $f_i = f_i^1 + f_i^2$, $\rho = \rho^1 + \rho^2$; $f_i^{eq}$ is an equilibrium function calculated at $\mathbf{u} = 0$ and $\rho$ by Eq. (10) (Zakirov et. al., 2018b):

$$f_i^{eq}(\rho,\mathbf{u}) = w_i\rho \cdot (1 + 3\frac{(\mathbf{e}_i \cdot \mathbf{u})}{c^2} + 4.5\frac{(\mathbf{e}_i \cdot \mathbf{u})^2}{c^4} - 1.5\frac{\mathbf{u}^2}{c^2}) \quad (10)$$

$\beta$ is a free parameter which controls a thickness of interface. It takes values from 0 to 1 and is equal to 0.8 in our study; $\alpha_i$ is an angle between **g** and $\mathbf{e}_i$ directions. Contact wetting angle is simulated using the approach described in (Akai et al., 2018).

### 2.2. Boundary and initial conditions

At the initial time, the pore space of flow domain on which the computational experiments are carried out is filled with a wetting fluid which has zero flow velocity. Both fluids have similar viscosity and density 1 m²/s and 1 g/cm³, respectively. A non-wetting phase is injected through the conventional left side of the region, perpendicular to the $OX$ axis, and is selected through the right side; the flow is occurred when the non-wetting fluid injected through the input boundary at known constant velocity. The pressure the output section is known and constant. Other external sides of the flow region are impermeable. In the LBE framework, the boundary conditions on the input and output boundaries are given by Zou and He relations (Zou, He, 1997). The boundary conditions on the impermeable obstacles are realized by "bounce-back" rule (Zakirov et. al, 2018b).

The implementation of mathematical model was in the form of software codes in Microsoft Visual Studio 2017 development environment using Intel Fortran programming language. The numerical validations of the algorithm on the layered flow in channel as well as on drainage displacement were preformed in (Zakirov et al., 2018a, 2018b).

### 2.3. Image processing and samples description

In this paper, sandstone from Ashalchinskoe oil field (Tatarstan, Russia) was used. The digital model of the pore space was formed on the base of X-ray computed tomography. The scans of cores were made on a micro-/nanofocus X-ray monitoring system for computed tomography and 2D inspection GE Phoenix v|tome|x s 240. We selected a cubic core with size of 3.7 millimeters for which X-ray tomographic scanning was performed. The resolution of digital model was 4.0 μm. Fig. 1 shows the X-ray CT 3D image with size of 350³ voxels.

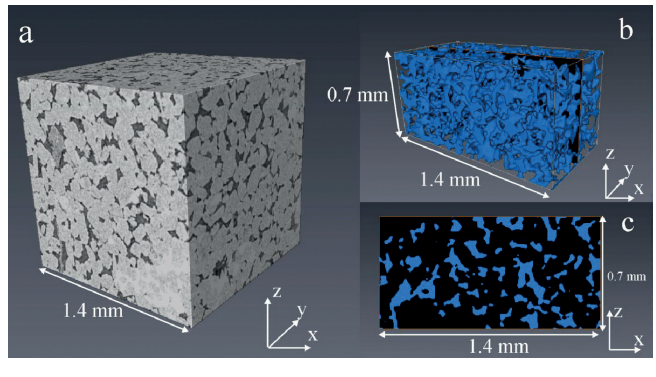


*Fig. 1. 3D Digital X-ray CT model of sandstone with resolution of 4 μm: a – 3D-image with size of 350³ voxels; b – 3D-pore space of subsample No. 1 with size of 350×175×175 voxels; c – 2D-slice perpendicular to OY direction*

The gray color scale in Fig. 1a characterizes the X-ray radiation attenuation intensity by different areas of the sample: light gray regions are the granules of sandstone, and black represents the pore space. Imaging of invasion processes, reported in sections 3.1, was carried out on subsample with smaller size of 250×125×125 voxels. Its porosity is 0.272 and $k_{XX}$ = 0.612 μm$^2$.

The statistical investigations of Haines jumps, reported in section 3.2, were conducted on four subsamples, cut from big model, with dimensions of 350×175×175 voxels. Their properties are given in Table 1. A porous structure of subsample No.1, which was extracted after binarization, is shown in Figs. 1b and 1c.

| Subsample number | Porosity, rel. units | Absolute permeability component $k_{XX}$, μm$^2$ |
|---|---|---|
| 1 | 0.270 | 0.645 |
| 2 | 0.263 | 0.456 |
| 3 | 0.277 | 0.621 |
| 4 | 0.276 | 0.541 |

*Table 1. The porosities and absolute permeability components $k_{XX}$ of four subsamples*

## 3. Results and discussion

### 3.1. Pore-scale invasion events and dynamic characteristics of the flow

The focus of this is to establish links between numerical dynamic characteristics of the flow. The computational experiment was carried out on subsample with dimension of 250×125×125 voxels at flow wate $u_0$ = 0.2×10$^{-3}$ m/s, surface tension $\sigma$ = 20 mN/m and contact wetting angle $\theta$ = 10°. Firstly, in Fig. 2, we show the pressure difference evolution in time between inlet and outlet boundaries of the flow domain (further, the pressure difference between boundaries will be denoted as $P$, and pressure drops which occur during Haines jumps will be indicated as $\Delta P$). The pressure measurement was made every 500 time steps which is equal to 0.08 ms. The blue curve in Fig. 2 shows the dynamics of $P$ in the absence of capillary forces ($\sigma$ (mN/m) = 0).

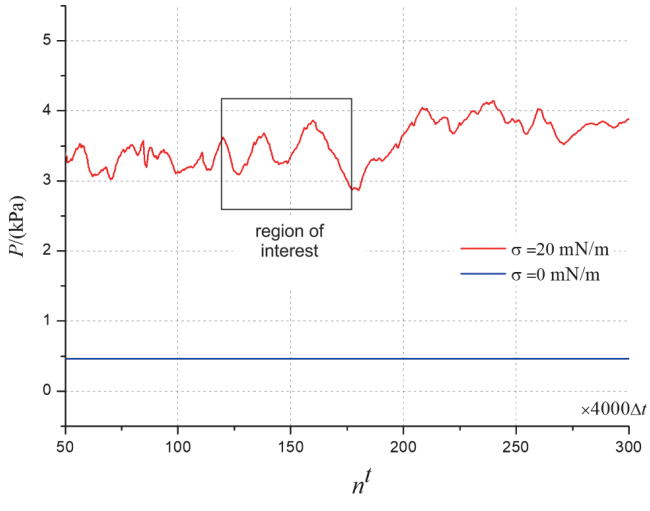


*Fig. 2. The dynamics of pressure difference between input and output boundaries of the sample during drainage displacement*

According to red curve in Fig. 2, the fluctuations of $P$ are observed and the dynamics has wavy behavior (see also Fig. 7). In addition, to determine the cause of pressure fluctuation and to strengthen the link between numerical dynamics characteristics and invasion events, the specific surface area of pore space $S_V$, occupied by invaded non-wetting fluid, was calculated. This characteristic is defined as the ratio between surface area of non-wetting fluid and its volume. Further, we will accent on a period from 115 to 175 of $n^t$ (the area of interest in Figs. 2 and 3). Fig. 3b shows the dynamics of change of the pore space specific surface area $\Delta S_V$, where $\Delta S_V(n^t+1) = S_V(n^t+1) - S_V(n^t)$.

Step-by-step imaging of pore-filling events is shown in Figs. 4-6. Fig. 4a illustrates the distribution of injected non-wetting phase, which corresponds to position "a" and to "event 1" in Fig. 3. The blue

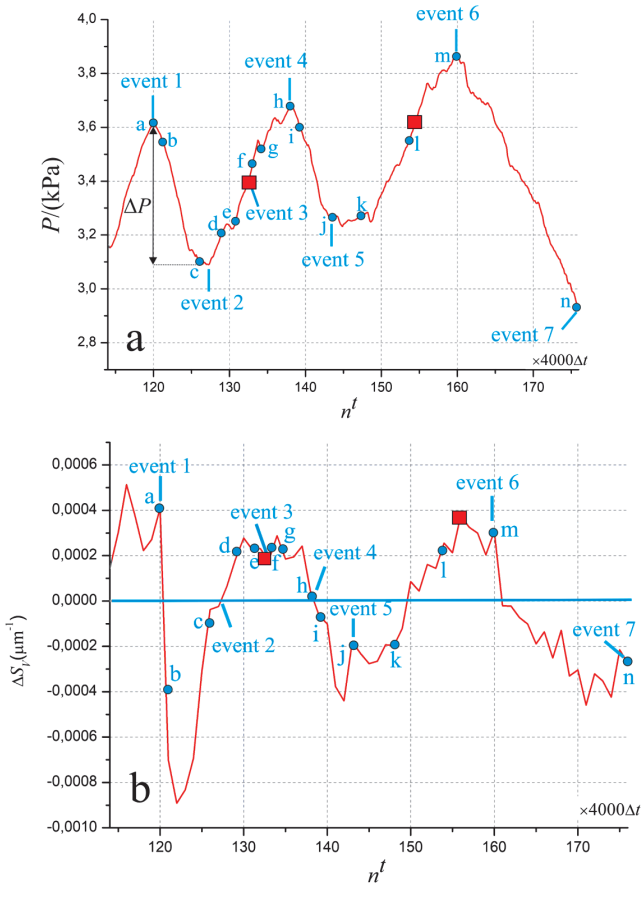


*Fig. 3. The dynamics of the flow characteristics in the interval $n^t$ = [115,175]: a – fluctuations of pressure difference; b – fluctuations of the change of the porous space specific surface area, which is occupied by non-wetting fluid. The "events" and positions "a" – "n", marked in graphs, are associated with Figs. 4-6. Red squares indicate the appearance of new mobile interfaces.*

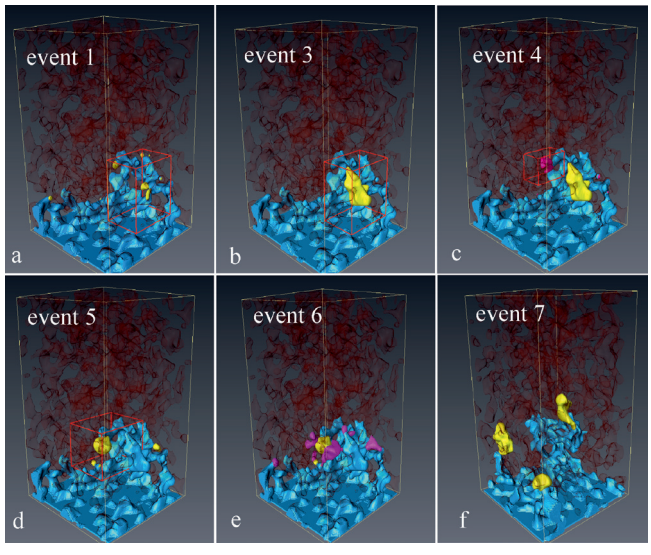


*Fig. 4. The distributions of non-wetting phase during displacement between "event 1" and "event 7" (Fig. 3). The invaded regions between current and previous events are shown in yellow and pink. Blue, yellow and pink – the non-wetting phase, dark red – pore space occupied by wetting fluid.*

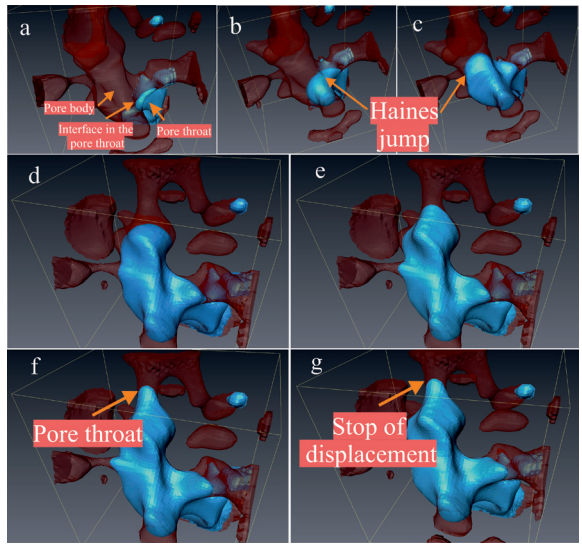


*Fig. 5. The dynamics of non-wetting phase displacement between "event 1" and "event 4" (Fig. 3) in red box shown in Fig. 6a: a – the meniscus location in the connection of the pore throat and its body, position "a"; b, c – the rapid invasion of non-wetting phase to the pore body (Haines jump), positions "b" and "c"; d, e – the finish of rapid invasion, the displacement of interface at narrowing of the pore size, positions "d" and "e"; f, g – the meniscus location in new pore throat and the stop of interface displacement in current pore channel, positions "f" and "g". Positions "a" – "g" are associated with Fig. 3. Blue – the non-wetting phase, dark red – pore space occupied by wetting fluid.*

color in Fig. 3a is a distribution of non-wetting phase at $n^t$ = 115, and yellow shows the non-wetting phase invaded during $n^t$ = [115, 120]. According to Fig. 3, the capillary pressure growth is accompanied by increase in the specific surface area because $\Delta S_V > 0$. Such relationship of the characteristics is explained by the inverse dependences of the specific surface and capillary pressure on the radius of the pore channel.

Next, after "event 1" in Fig. 3a, a pressure drop $\Delta P$ was detected. Drainage events in the interval between "event 1" and "event 3" will occur in a region of red box shown in Figs. 4a and 4b. Fig. 5 illustrates these events in larger view. The location of liquids interface in narrow pore throat, which will move in next snapshot to wide pore body, is shown in Fig. 5a (position "a" in Fig. 3). The reason of drainage event in this region is the pressure difference exceeding of the capillary pressure of this meniscus. Figs. 5b and 5c illustrate the invasion for positions "b" and "c" (Fig. 3). According to them, an observed event, when drainage front displaced, occurs rapidly and looks as a burst-like flow. Rapid invasion process is due to the sharp growth of pore channel size during meniscus displacement from pore throat to its body. This observation is also in agreement with variation of the specific surface area. According to Fig. 3b, the rapid increase in the interface surface between positions "a" and "c" is detected. Such character of the interface displacement is reflected and associated with quick drop of capillary pressure. The described phenomenon is a Haines jump.

Figs. 5d and 5e show meniscus displacement in positions "d" and "e". The drainage process continues in the same pore-channel and absent in the other regions of the pore space. It can be noted that after finish of rapid invasion from pore throat to its body, we detected the growth in capillary pressure in Fig. 3a after "event 2". According to Figs. 5d and 5e, the reason of such increase is the decrease in meniscus radius due to narrowing of the pore size on its pathway, which is also supported by Fig. 3b ($\Delta S_V > 0$ in interval between positions "c" and "e"). Fig. 4b shows the distribution of non-wetting phase in "event 3". The region occupied by non-wetting phase between "event 1" and "event 3" is shown in yellow.

Due to decrease in mobile interface radius, the probability of new invaded regions appearance is growing. Drainage process will continue in pore channel where capillary resistance, produced by meniscus, is lower than in current mobile interface. Figs. 5f and 5g (positions "f" and "g" in Fig. 5) illustrate finish of invasion event in this pore channel. The switching of mobile interface occurs between positions "e" and "f" and corresponds to "event 3". Fig. 3 shows that in this time interval, the increase in capillary pressure and specific surface area is observed. The new invaded region in "event 4" is shown in Fig. 4c. The area occupied by non-wetting phase between "event 3" and "event 4" is shown in pink in new red box.

Next, new drainage displacement between "event 4" and "event 5" (Fig. 3), as can be seen in Fig. 4d, will occur in a region of red box. Fig. 6 illustrates the invasion events in this time interval in a larger view.

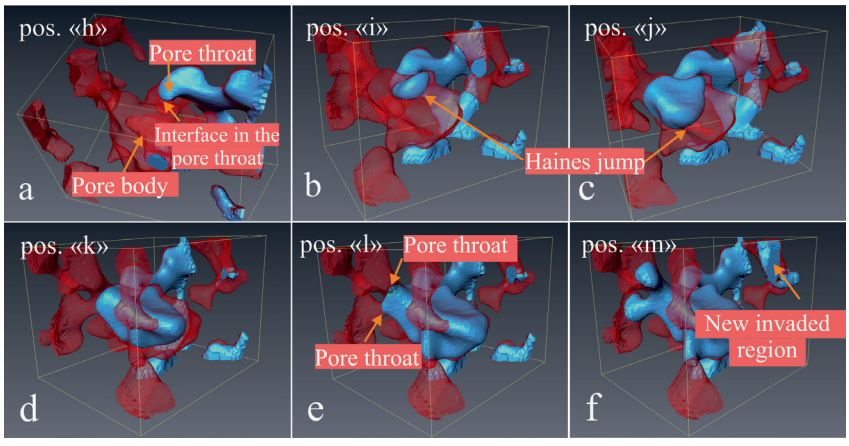


*Fig. 6. The dynamics of non-wetting phase displacement between "event 4" and "event 6" (Fig. 3) in red box shown in Fig. 4d: a – the meniscus location in the connection of the pore throat and its body, position "h"; b, c – Haines jump, positions "i" and "j"; d – f – the finish of rapid invasion, the following uniform displacement at narrowing of the pore size and the appearing of new mobile interface, positions "k" – "m". Positions "h" – "m" are associated with Fig. 3. Blue – the non-wetting phase, dark red – pore space occupied by wetting fluid.*

In position "h" (Fig. 3), shown in Fig. 6a, the interface is located in pore throat, and the pressure difference, evidently, exceeds capillary resistance of meniscus because followed event, which is illustrated in Figs. 6b and 6c, will occur in this pore channel. Haines jump is observed in positions "i" and "j" and associated with sharp decrease in capillary pressure and specific surface area (Fig. 3). The region occupied by non-wetting fluid between "event 4" and "event 5" is shown in yellow in Fig. 4d.

"Event 5" in Fig. 3 corresponds to the finish of Haines jump and appearance of new mobile interfaces. Invasion events, as shown in Figs. 6d and 6e (positions "k" and "l" in Fig. 3), will continue in current pore, but at narrowing of meniscus size. The displacement after position "j" and before "m" occurs uniformly and at growth of capillary pressure and specific surface area (Fig. 3). The pore space filled by non-wetting phase between "event 5" and "event 6" is shown in pink in Fig. 4e.

Next, we detected a sharp drop of capillary pressure and specific surface area after "event 6" (Fig. 3), again. According to established association between invasion events and dynamics of capillary pressure and specific surface area, Haines jumps were expected after "event 6" and they really were observed between positions "m" and "n" (Fig. 3). The regions invaded between "event 6" and "event 7" are shown in yellow in Fig. 4f.

It should be stressed that, in general case, the switching of mobile interfaces and/or the continuation of displacement in current pore after Haines jump is a result of the "competition" of capillary pressures produced by current mobile interface and other static meniscus. Thus, the revealed change of the mobile interfaces, along with Haines jump, is another new distinctive feature of the capillary forces dominance.

So, based on obtained in this section results, we can note that the scenario of drainage displacement with the dominance of capillary forces consists of following stages: 1 – uniform invasion in narrow pore channels at growth of capillary pressure and specific surface area; 2 – rapid invasion event during Haines jump and sharp drop of capillary pressure and specific surface area; 3 – finish of Haines jump and continuation of uniform invasion in current pore, where Haines jump occurred, the resumption of increase in capillary pressure and specific surface area; 4 – appearance of new mobile interfaces in other regions of pore space or continuation of uniform invasion in current pore in general case; 5 – Haines jump in new region of pore space. The sequence of stages 2-4 can be considered as a period of drainage events which, according to Figs. 2 and 7, will be repeated with variation of the time duration and amplitude of the pressure fluctuations.

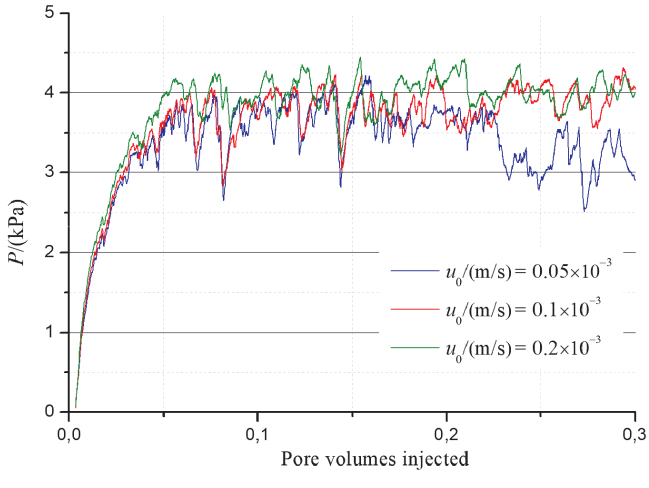


*Fig. 7. The dynamics of pressure difference during drainage displacement for different injected fluid velocities*

### 3.2. Haines jumps statistics

In this section, we investigate the impact of flow rate and surface tension on statistical distributions of pressure

drops at Haines jumps. It should be noted that, despite 2D micromodels, the statistical investigations on 3D X-ray CT images are limited and hampered. One of the reasons is a high resolution of digital model and, consequently, its small pore volume and large grid dimension, which is also accompanied by big computational costs. Thus, the number of pore-scale events in 3D models is less than in 2D micromodels (more than 500 (Furuberg et al., 1996; Soto et al., 2017)). Also, the investigation on big pore volumes is hampered with simultaneous invasion events, whereas it's necessary to observe the individual processes for statistical interpretation. That is why, for decreasing the frequency of simultaneous Haines jump and to obtain the sufficient number of pressure drops, the numerical experiments were conducted on four subsamples, which properties are given in Table 1.

### 3.2.1. Effect of flow rate

For the flow rate affect investigation, the series of numerical experiments at wide range of the injected fluid velocity was carried out: [0.05÷1.5]×10$^{-3}$ m/s. The surface tension in all simulations was 20 mN/m. The *Ca* numbers and average estimations of the relations between capillary pressure ($P^{cap}$) and pressure difference between input and output sections of the subsamples, conditioned by viscous forces action ($P^{visc}$), are given in Table 2. All simulations were carried till injection of 0.3 pore volumes.

The dynamics of pressure difference for subsample No.2, plotted for three cases of flow rate, is shown in Fig. 7. According to shown in column 5 (Table 2) data, the number of detected pressure drops ($N^{drop}$) is strongly affected by the flow rate. This feature is clearly visible on Fig. 7. We must note that $N^{drop}$ is not equal to the number of individual Haines jumps. It was revealed that increase in injected fluid velocity leads to the growth of the mobile interfaces number. Thus, the number of simultaneous Haines jumps will increase with the magnitude of the flow rate and most individual jumps, especially at high velocities, cannot be separated and distinguished during a single pressure drop.

When imaging of invasion processes, it was found that for $u_0 \geq 0.4\times10^{-3}$ m/s, three and more simultaneous jumps occur during single pressure drop, whereas for $u_0 \leq 0.2\times10^{-3}$ m/s, the number of simultaneous jumps during single pressure drop doesn't exceed two. Such feature makes impossible strict statistical investigation for $u_0$/(m/s) $\geq 0.4\times10^{-3}$.

For $u_0 = 0.2\times10^{-3}$ m/s, the proportion of simultaneous paired jumps during single pressure drop is about 30 % and decreases to 5 % for $u_0 = 0.05\times10^{-3}$ m/s. Therefore, the influence of flow rate on the individual jumps number exists but insignificant. This observation is also reinforced with calculated pore volume filled during pressure drops ($PV^{jump}$ in column 7, Table 2). According to shown in column 7 data, $PV^{jump}$ values for $u_0 \leq 0.2\times10^{-3}$ m/s are almost the same.

The statistical distributions of pressure drops for $u_0 \leq 0.2\times10^{-3}$ m/s are shown in Fig. 8. It was revealed that obtained distributions obey lognormal law with R-squared equal to 0.93, 0.96 and 0.94 in the order of increasing $u_0$. According to Fig. 8, the flow rate affect on statistical distribution is insignificant, but influences on the mean value of pressure drop $\Delta\overline{P}$.

According to numerous experiments on 2D and 3D micromodels in (Moebius, Or, 2012; Furuberg et al., 1996; Soto et al., 2017), the cumulative distribution *N* of pressure drops obeys following relation:

$$\ln(N) = \beta \cdot \Delta P / \Delta\overline{P} \quad (11)$$

where $\beta$ is the linear coefficient. Fig. 8b shows the cumulative distribution *N*. The solid lines in Fig. 8b are the approximating curves using Eq. (11) with R-squared exceeding 0.98. Thus, the pressure drops statistics in 3D heterogeneous models of porous media, in 2D granular homogenous models (Moebius, Or, 2012; Furuberg et al., 1996) and in macroporous soils (Soto et al., 2017) obey the same law. When approximating the cumulative distribution, it was calculated that the $\beta$ coefficients are –0.970, –0.983, –0.969 in the order of increasing $u_0$. Such close values indicate on the weak influence of flow rate on the statistical distributions of pressure drops.

### 3.2.2. Effect of surface tension

For the investigation of the surface tension affect, a series of numerical experiments at $\sigma$ = 13, 20 and 28 mN/m was carried out. $u_0 = 0.1\times10^{-3}$ m/s in all simulations. All simulations were carried till injection of 0.3 pore volumes.

| No. | $u_0\times10^{-3}$, m/s | $log_{10}Ca$ | $P^{cap}/P^{visc}$ | $N^{drop}$ | Mean value $\Delta\overline{P}$, kPa | $PV^{jump}$ |
|---|---|---|---|---|---|---|
| 1 | 0.05 | -5.6 | 67 | 360 | 0.206 | 0.265 |
| 2 | 0.1 | -5.3 | 33.5 | 307 | 0.173 | 0.252 |
| 3 | 0.2 | -4.9 | 16.7 | 271 | 0.165 | 0.257 |
| 4 | 0.4 | -4.7 | 8.3 | 193 | 0.152 | 0.266 |
| 5 | 0.8 | -4.4 | 4.2 | 159 | 0.129 | 0.256 |
| 6 | 1.5 | -4.1 | 2.0 | 119 | 0.111 | 0.247 |

*Table 2. The numerical values of computational simulations and the results of the flow rate affect on pressure drops statistics*

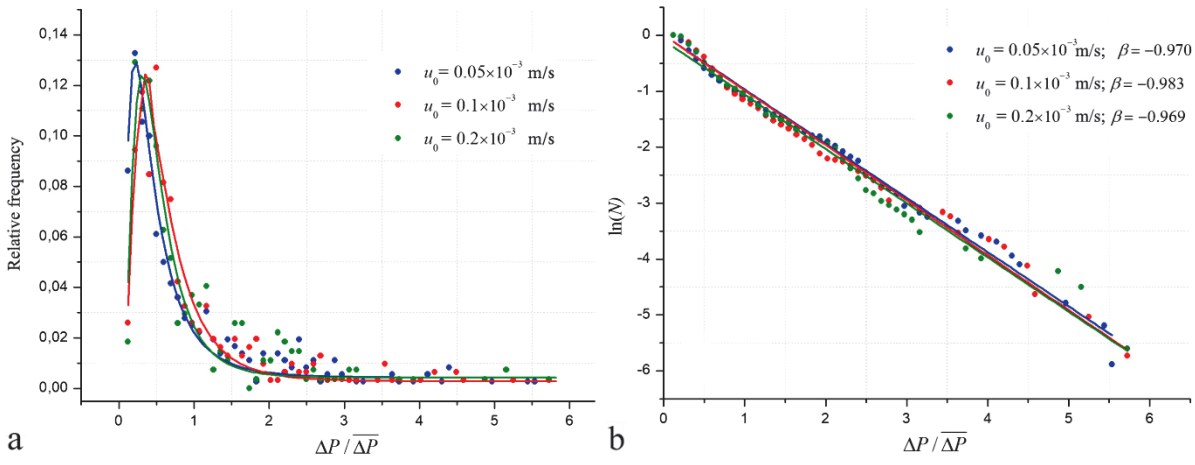


*Fig. 8. The statistical distributions of the dimensionless parameter $\Delta P / \Delta \overline{P}$, calculated for different injected fluid velocities: a – distributions in form of the relative frequency; b – the cumulative distributions N. The circle symbols show measured data, and the solid lines are the result of approximation.*

The characteristics of numerical simulations are given in Table 3. According to shown data, the value of interfacial interaction practically does not influence on the number of pressure drops (column 5, Table 3), but affects on its magnitude (column 6, Table 3). The close values of $PV^{jump}$ (column 7, Table 3) indicate on the weak influence on the number of individual Haines jumps.

Fig. 9 illustrates the distributions of pressure drops at various surface tensions. Solid lines in Fig. 9 are the result of approximation by lognormal law. The R-squared for each curve exceed 0.93. The character of solid lines in Fig. 9 indicates a weak surface tension influence on the statistical distributions.

Thus, taking to account that $\beta \approx -1$ regardless of the injected fluid velocity and surface tension, it can be supposed that the statistical distribution of $\Delta P / \Delta \overline{P}$ is determined only by the geometry of porous structure. For example: $\beta = -1.3$ and $-1.5$ for two types of 2D mircomodels and $\beta = -1.7$ for 3D granular model in (Moebius, Or, 2012); $\beta = -1.31$ for 2D model in (Furuberg et al., 1996); $\beta \approx -3$ for soils in (Soto et al., 2017). This assumption requires special investigations in future.

| No. | $\sigma$ mN/m | $log_{10}Ca$ | $P^{cap}/P^{visc}$ | $N^{drop}$ | Mean value $\Delta \overline{P}$, kPa | $PV^{jump}$ |
|---|---|---|---|---|---|---|
| 1 | 13 | -5.1 | 21.7 | 289 | 0.115 | 0.268 |
| 2 | 20 | -5.3 | 33.5 | 307 | 0.173 | 0.252 |
| 3 | 28 | -5.45 | 47 | 300 | 0.241 | 0.278 |

*Table 3. The numerical values of computational simulations and the results of the surface tension affect on pressure drops statistics*

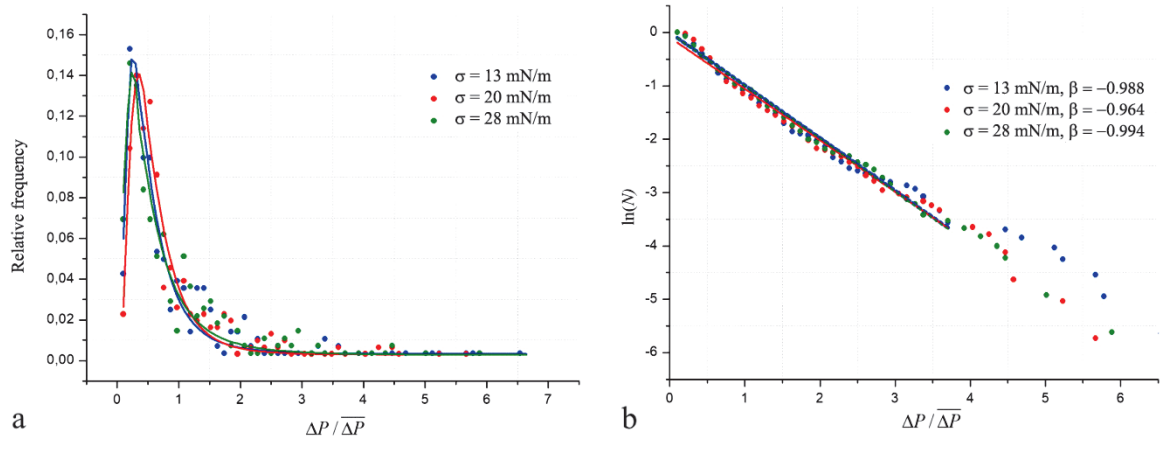


*Fig. 9. The statistical distributions of the dimensionless parameter $\Delta P / \Delta \overline{P}$ calculated for different surface tensions: a – distributions in form of relative frequency; b – the cumulative distributions N. The circle symbols show measured data, and the solid lines are the result of approximation.*

## Conclusion

In this paper, we investigated the effects which occur during two-phase flow in natural 3D model of porous media with the dominance of capillary forces. A sequence of events has been identified that can be considered a period of drainage displacement. It consists of the following steps: Haines jump; continuation of the displacement in this channel, where a jump occurred; the appearance of new mobile menisci and subsequent displacement in new regions of the pore space. Periodic switching of moving interfaces is a new distinctive feature of the capillary forces manifestation in a porous medium.

The statistical investigations of pressure drops, which occur at Haines jumps, show that their distribution obeys lognormal law. It was found that the parameters of two-phase flow don't influence on the statistical distribution of pressure drops and affect only on its magnitude.

## Acknowledgements

*The work is performed according to the Russian Government Program of Competitive Growth of Kazan Federal University and by RFBR according to the research project No. 18-31-00134.*

*The authors are grateful to the reviewer for valuable comments that contributed to the improvement of the article.*

## References

Akai T., Bijeljic B., Blunt M.J. (2018). Wetting boundary condition for the color-gradient lattice Boltzmann method: Validation with analytical and experimental data. *Advances in Water Resources*, 116, pp. 56-66. https://doi.org/10.1016/j.advwatres.2018.03.014

Armstrong R.T., Berg S. (2013). Interfacial velocities and capillary pressure gradients during Haines jumps. *Physical Review E*, 88, 043010. https://doi.org/10.1103/PhysRevE.88.043010

Armstrong R.T., Evseev N., Koroteev D., Berg S. (2015). Modeling the velocity field during Haines jumps in porous media. *Advances in Water Resources*, 77, pp. 57-68. https://doi.org/10.1016/j.advwatres.2015.01.008

Aursjø O., Løvoll G., Knudsen H.A., Flekkøy E.G., Måløy K.J. (2011). A Direct Comparison Between a Slow Pore Scale Drainage Experiment and a 2D Lattice Boltzmann Simulation. *Transport in Porous Media*, 86(1), pp. 125-134. https://doi.org/10.1007/s11242-010-9611-y

Chen Y.-F., Wu D.-S., Fang Sh., Hu R (2018). Experimental study on two-phase flow in rough fracture: Phase diagram and localized flow channel. *International Journal of Heat and Mass Transfer.* 122, pp. 1298-1307. https://doi.org/10.1016/j.ijheatmasstransfer.2018.02.031

Furuberg L., Maløy K.J., Feder J. (1996). Intermittent behavior in slow drainage. *Physical Review E*, 53, pp. 966-977. https://doi.org/10.1016/0378-4371(92)90542-X

Haines W.B. (1930). Studies in the physical properties of soil. *Journal of Agricultural Science*, 20, pp. 98-116. https://doi.org/10.1017/S002185960008864X

Leclaire S., Parmigiani A., Malaspinas O., Chopard B., Latt J. (2017). Generalized three-dimensional lattice Boltzmann color-gradient method for immiscible two-phase pore-scale imbibition and drainage in porous media. *Physical Review E*, 95, 033306. https://doi.org/10.1103/PhysRevE.95.033306

Liu H., Kang Q., Leonardi C.R., Schmieschek S., Narváez A., Jones B.D., Williams J.R., Valocchi A.J., Harting J. (2016). Multiphase lattice Boltzmann simulations for porous media applications. *Computational Geosciences*, 20(4). pp. 777-805. https://doi.org/10.1007/s10596-015-9542-3

Moebius F., Or D. (2012). Interfacial jumps and pressure bursts during fluid displacement in interacting irregular capillaries. *Journal of Colloid and Interface Science*, 377, pp. 406-415. https://doi.org/10.1016/j.jcis.2012.03.070

Moebius F., Or D. (2014). Pore scale dynamics underlying the motion of drainage fronts in porous media. *Water Resources Research*, 50, pp. 8441-8457. https://doi.org/10.1002/2014WR015916

Soto D., Paradelo M., Corral Á., López Periago J.E. (2017) Pressure jumps during drainage in macroporous soils. *Vadose Zone Journal*, 16. https://doi.org/10.2136/vzj2017.04.0088

Tsuji T., Jiang F., Christensen K.T. (2016). Characterization of immiscible fluid displacement processes with various capillary numbers and viscosity ratios in 3D natural sandstone. *Advances in Water Recourses*. 95, pp. 3-15. https://doi.org/10.1016/j.advwatres.2016.03.005

Yamabe H., Tsuji T., Liang Y., Matsuoka T. (2015). Lattice Boltzmann Simulations of Supercritical CO2−Water Drainage Displacement in Porous Media: CO2 Saturation and Displacement Mechanism. *Environmental Science and Technology*, 49, pp. 537-543. https://doi.org/10.1021/es504510y

Zacharoudiou I., Boek E.S. (2016). Capillary filling and Haines jump dynamics using free energy Lattice Boltzmann simulations. *Advances in Water Resources*, 92, pp. 43-56. https://doi.org/10.1016/j.advwatres.2016.03.013

Zakirov T.R., Galeev A.A., Statsenko E.O., Khaidarova L.I. (2018a). Calculation of filtration characteristics of porous media by their digitized images. *Journal of Engineering Physics and Thermophysics*, 91(4), pp. 1069-1078. https://doi.org/10.1007/s10891-018-1833-9

Zakirov T.R., Galeev A.A., Khramchenkov M.G (2018b). Pore-scale Investigation of Two-Phase Flows in Three-Dimensional Digital Models of Natural Sandstones. *Fluid Dynamics*. 53(5), pp. 76-91. https://doi.org/10.1134/S0015462818050087

Zou Q., He X. (1997). On pressure and velocity boundary conditions for the lattice Boltzmann BGK model. *Phys. Fluids*, 9, pp. 1591-1598. https://doi.org/10.1063/1.869307

## About the Authors

*Timur R. Zakirov* – Cand. Sci. (Physics and Mathematics), Associate Professor, Institute of Geology and Oil and Gas Technologies, Kazan Federal University

18, Kremlevskaya st., Kazan, 420008, Russian Federation

E-mail: tirzakirov@kpfu.ru

*Maxim G. Khramchenkov* – Dr. Sci. (Physics and Mathematics), Professor, Head of the Department of Mathematical Methods in Geology, Kazan Federal University; Leading Researcher, Scientific Research Institute for System Analysis of the Russian Academy of Sciences

18, Kremlevskaya st., Kazan, 420008, Russian Federation

*Manuscript received 16 August 2019;*
*Accepted 25 October 2019;*
*Published 30 March 2020*